Journal of
Materials Chemistry C

Accepted Manuscript

This article can be cited before page numbers have been issued, to do this please use: J. Feng, H. Dong, L. Yu and L. Dong, *J. Mater. Chem. C*, 2017, DOI: 10.1039/C7TC00631D.

ROYAL SOCIETY OF CHEMISTRY

rsc.li/materials-c

View Article Online
DOI: 10.1039/C7TC00631D

Journal Name

ARTICLE

Optical and Electronic Properties of Graphene Quantum Dots with Oxygen-Containing Groups: a Density Functional Theory Study

Received 00th January 20xx,
Accepted 00th January 20xx

DOI: 10.1039/x0xx00000x

www.rsc.org/

Jianguang Feng,[a*] Hongzhou Dong,[a] Liyan Yu,[a*] and Lifeng Dong [a, b*]

Effects of five types of oxygen-containing functional groups (-COOH, -COC-, -OH, -CHO, and -OCH_3) on graphene quantum dots (GQDs) are investigated using time-dependent density functional theory (TD-DFT). Their absorption spectra and HOMO–LUMO gaps are quantitatively analyzed to reveal the influence of different oxygen-containing groups including their locations and quantities on optical properties of GQDs. Compared with those on the edge of GQD plane, oxygen-containing groups located on the surface have more evident effects on optical properties. The calculated HOMO–LUMO gaps of pristine GQDs and edge-functionalized GQDs with -OH, -COOH, -OCH_3, -CHO, and -COC- are 2.34, 2.32, 2.31, 2.30, 2.27, and 2.15 eV, respectively, whereas the HOMO–LUMO gaps of surface-functionalized GQDs with the groups above are 0.36, 0.32, 0.37, 0.39, and 1.86 eV, respectively. Interestingly, the influence of surface and edge functionalization on the HOMO–LUMO gap of GQDs is almost opposite. The absorption process is investigated along with excited state analysis, which includes the oscillator strengths, natural transition orbital, and charge difference density . It is found that functionalization on the basal plane greatly change the distribution of electron density in surface-functionalized GQDs.

Introduction

Graphene is one atomic layer in thickness with carbon atoms arranged in a two-dimensional honeycomb crystal lattice. Since its discovery in 2004, graphene has demonstrated excellent chemical and physical properties and broad potential applications.[1-4] Since graphene has zero-band gap, the possibility for observing its photoluminescence (PL) is impossible, which strongly limits its applications in optoelectronics and photonics.[5, 6] However, the problem of zero-band gap can be solved by reducing the lateral dimensions of graphene into nanoribbons or quantum dots (QDs).[7, 8] Due to quantum confinement[9] and edge effects,[10] zero-dimensional GQDs have demonstrated excellent optical, unique electronic, and stable PL properties for bright potential applications in optoelectronics,[11-13] bioimaging,[14] and light emission.[15]

Successful strategies for synthesizing GQDs with tunable properties can be divided into two methods: top-down and bottom-up approaches. The top-down is to directly cut graphene sheet such as large graphene, graphene oxide and carbon nanotubes into quantum dots through a series of physical, chemical, and electrochemical techniques, which include acidic oxidation,[16-18] hydrothermal[19, 20] and solvothermal[21, 22] cutting, electrochemical scissoring,[23, 24] chemical exfoliation,[6, 17] and ultrasonic shearing.[25] For the bottom-up method, GQDs can be controllably prepared through solution chemistry, cyclodehydrogenation of polyphenylene precursors,[26] or carbonizing some special organic precursors via chemical synthesis.[27-29] The top-down route for the preparation of GQDs has the advantages of abundant raw materials, large-scale production, and simple operation. However, the GQDs synthesized via top-down methods usually contain oxygen-containing functional groups (OCFGs) including hydroxyl (-OH), epoxy (-O-), ether(-OCH_3), carbonyl (-(C=O)), and carboxyl (-COOH) groups.[30] For instance, the GQDs prepared from carbon fibers via acidic oxidation were functionalized with hydroxyl, carbonyl, and carboxylic acid groups.[17] The interlayer distance of GQDs is broader than that of carbon fibers and graphite, which results from oxygen-containing groups introduced into the edges, interfaces, and surfaces of GQDs during the oxidation. These OCFGs can facilitate the solubility and increase specific surface area, while they may change optical and electronic properties of GQDs. Wang et al. synthesized GQDs by solvothermally cutting graphene oxide, and revealed that functional groups (such as carboxyl and carbonyl groups) on the edge of GQDs contribute to green PL emission of GQDs.[31, 32] Hamilton et al. demonstrated orientation control of GQDs on polar surfaces through chemical functionalization with desirable oxygen-containing group -COOH.[33] Zhu et al. developed a method to tune the PL of GQDs through surface chemistry and claimed that carbonyl, epoxy, and amide moieties were changed into

[a] College of Materials Science and Engineering, Qingdao University of Science and Technology, Qingdao 266042, China (Email: DongLifeng@qust.edu.cn, LiyanYu@qust.edu.cn, and fengjg@qust.edu.cn).
[b] Department of Physics, Hamline University, St. Paul 55104, USA (Email: ldong03@hamline.edu).
†Electronic Supplementary Information (ESI) available: [details of any supplementary information available should be included here]. See DOI: 10.1039/x0xx00000x

View Article Online
DOI: 10.1039/C7TC00631D

hydroxyl groups during a reduction process, thereby suppressing non-radiative process and enhancing the integrity of π-conjugated system.[34] Zhu et al. obtained GQDs with controllable surface oxidation by hydrazine hydrate reduction and found that GQDs had tunable fluorescence induced by the degree of surface oxidation.[20]

GQDs prepared via various methods have demonstrated different properties, including size,[17] solvent polarity,[10] surface oxidation degree,[34] and surface functionalization.[35] Nevertheless, effects of each factor above on certain properties can be separately investigated through theoretical calculations. Schumacher et al. studied theoretical structural and electronic properties of the ground state and absorption spectral characteristics of GQDs containing 168 conjugated carbon atoms in gas phase. They elucidated on optical selection rules in isolated GQDs and their relation to the system symmetry and brought general results into a broader context with other semiconductor systems.[36] Zhao et al. studied absorption and fluorescence spectra of GQDs, and bulk solvent effects were taken into consideration by using polarizable continuum model (PCM). They found that the PL wavelengths of edge-functionalized C132 and C168 GQDs (contained 132 and 168 conjugated carbon atoms, respectively) red shifted when compared with that of pristine GQDs.[37] Geethalakshmi et al. evaluated the effect of hydroxyl functionalization on ionization potentials, light absorption and emission properties of graphene oxide quantum dots (GOQDs) through theoretical simulations, and optical properties of GOQDs were analyzed based on size and distribution of hydroxyl functional groups.[38] Li et al. studied electronic and optical properties of edge-functionalized GQDs utilizing density functional and many-particle perturbation theories.[39] They revealed that functional groups containing carbon–oxygen double bond (C=O) have advantages over the other groups in tuning electronic and optical properties of GQDs due to small charge transfer and large frontier orbital hybridization.

As discussed above, experimental and theoretical studies have shown that OCFGs can play a predominant role in optical and electronic properties of GQDs. However, it is usually quite difficult to conduct experiments to elucidate the detailed mechanism in each case. Besides, GQDs prepared via various methods possess different functional groups, which results in different optical and electronic properties. Therefore, a full understanding of GQDs mechanism is highly urgent, which can guide the synthesis of GQDs with expected properties. Considering that optical and electronic properties of C132 and certain functionalized C132 GQDs in different solvents have been studied experimentally and theoretically, in this study, we systematically investigated effects of five types of OCFGs on optical and electronic properties of C132 GQDs including their location (edge vs. surface) and quantity. The findings will guide the design and synthesis of GQDs for their optoelectronic and optical applications, such as optoelectronic devices, sensors, and bioimaging.

Models and methods

As shown in Fig. 1, a series of functionalized C132 GQDs are investigated. Five oxygen-containing groups, carboxyl (-COOH), epoxy (-COC-), hydroxyl (-OH), aldehyde (-CHO), and ether ($-OCH_3$), are added to form bonds with carbon atoms from the basal plane and substitute hydrogen atoms of the edge plane. For simplicity, surface- and edge-functionalized GQDs are denoted as C132-RN-SF and C132-RN-EF, respectively, where R indicates the functional group and N represents the number of functional group. Recently, time-dependent density functional theory (TD-DFT)[40] and PCM[41] were utilized for excited-state optimization with the inclusion of bulk solvent effects.[42] Many PCM/TD-DFT computational studies gave good results compared with experimental values.[37, 43, 44] Therefore, the PCM/TD-DFT approach is utilized to explore detailed optical properties of GQDs with oxygen-containing groups.

Geometry optimizations for the ground states of GQDs are first calculated by DFT with the Becke three-parameter Lee–Yang–Parr hybrid functional (B3LYP) and 6-31G* basis set (B3LYP/6-31G*).[36] After the optimizations, TD-DFT calculations are performed to obtain vertical excitations of GQDs in the optimized ground state geometry with the same level of theory. A minimum of the first 20 lowest excited states are considered in all calculations. Due to the OCFGs, the GQDs are highly soluble in water.[17] Thus, all calculations in this work are conducted for GQDs in water. The solvent was included based on the PCM. For both calculations, quantum chemical modules implemented in Gaussian09 software[45] are employed. The dangling carbon bonds are passivated by hydrogen atoms. Visualizations of molecular orbitals and electron densities are done with GaussView, version 5[46].

Results and Discussion

Table 1 Calculated absorption maximum wavelengths for GQDs by PCM/TD-DFT-B3LYP/6-31G*.

GQDs	Wavelengths (nm)	
	Cal.	Exp.
C24	304.86	305[47]
C32	341.04	349[48]
C40	363.60	360[48]
C132	559.83	535[26]

The predictive applicability of the theoretical model should be tested to find its application scope. When dealing with specific microscopic structures and macroscopic properties of GQDs, the best way to test the method is to compare the calculations with their corresponding experimental data directly. Table 1 lists the calculated absorption maximum λ_{max} of pristine C24, C32, C40, and C132 GQDs (containing 24, 32, 40, and 132 conjugated carbon atoms, respectively) with different sizes and shapes compared with their corresponding experimental data. The structures of C24, C32, and C40 GQDs are shown in Fig. S1 of Supplementary Information (SI). The calculated maximum absorption wavelengths are in good agreement with available experimental data, which indicates

View Article Online
DOI: 10.1039/C7TC00631D

the selected theoretical mode is appropriate to describe the adsorption process of GQDs.

The calculated absorption spectra of pristine and functionalized C132 GQDs in water are given in Fig. 1. The absorption energy, wavelengths, and oscillator strengths for the first 20 lowest excited states of GQDs are listed in Tables S1–S11 in SI. The calculated absorption maximum λ_{max} of pristine C132 GQDs in water is 559.83 nm. In comparison, oxygen-containing groups can cause red shift of absorption characteristics of GQDs. The calculated absorption maximums λ_{max} of edge-functionalized GQDs with -OH, -OCH_3, -COOH, -CHO, and -COC- are 567.90, 572.11, 573.46, 585.08, and 601.53 nm, respectively. As shown in Fig. 1c, the optical absorption peaks of edge-functionalized GQDs with oxygen-containing groups only slightly red shift. The -COOH group enhances the absorption intensity of GQDs, while the -COC- reduces the intensity obviously. On the other hand, optical properties of surface-functionalized GQDs with oxygen-containing groups are significantly changed by surface functionalization, as shown in Fig. 1d. The calculated absorption maximums λ_{max} of surface-functionalized GQDs with -COC-, -OH, -OCH_3, -COOH, and -CHO are 556.63, 736.51, 734.07, 861.00, and 874.74 nm, respectively. The absorption intensity of surface-functionalized GQDs is greatly decreased. Notably, the C132-COC2-SF has the strongest adsorption intensity in surface-functionalized GQDs, but the calculated absorption maximum λ_{max} almost does not change. This indicates that oxygen-containing groups located on the surface plane have multiple effects on optical properties, while substitutions on the edge plane have limited impact. As we know, optical properties of GQDs are intimately associated with their electronic structures. This phenomenon may be attributed to the remarkable change of the electronic structures due to oxygen-containing groups located on the surface plane. It is essential to investigate how the number of oxygen-containing groups influences optical property of GQDs. In Fig. 1e, we choose -COOH groups as an example, and find that calculated absorption spectra tend to blue shift when the number of oxygen-containing groups decreases in functionalized GQDs, which is consistent with experimental investigations.[32] In particular, compared with pristine GQDs, the functionalized GQDs with eight -COOH groups on the surface plane have negligible absorption intensity. Thus, we only consider surface-functionalized GQDs with two oxygen-containing groups in this work.

Since the optical properties of GQDs are size and shape dependent, the pristine C24, C32, and C40 GQDs are selected to reveal the mechanisms underlying tunable optical and electronic properties of GQDs with different sizes and shapes. In addition, the -COOH and -COC- are chosen to study adsorption spectra of edge- and surface-functionalized C24–C40 GQDs. The details of results are given in Fig S1 and S2 (SI). It is found that the absorption spectra of functionalized C24–C40 GQDs have a red shift as compared to the pristine GQDs, and edge-functionalized GQDs have a small change in optical properties whereas a large change occurs when the basal planes of GQDs are modified. Hence, the conclusions for C24–C40 GQDs are consistent with that for C132 GQDs.

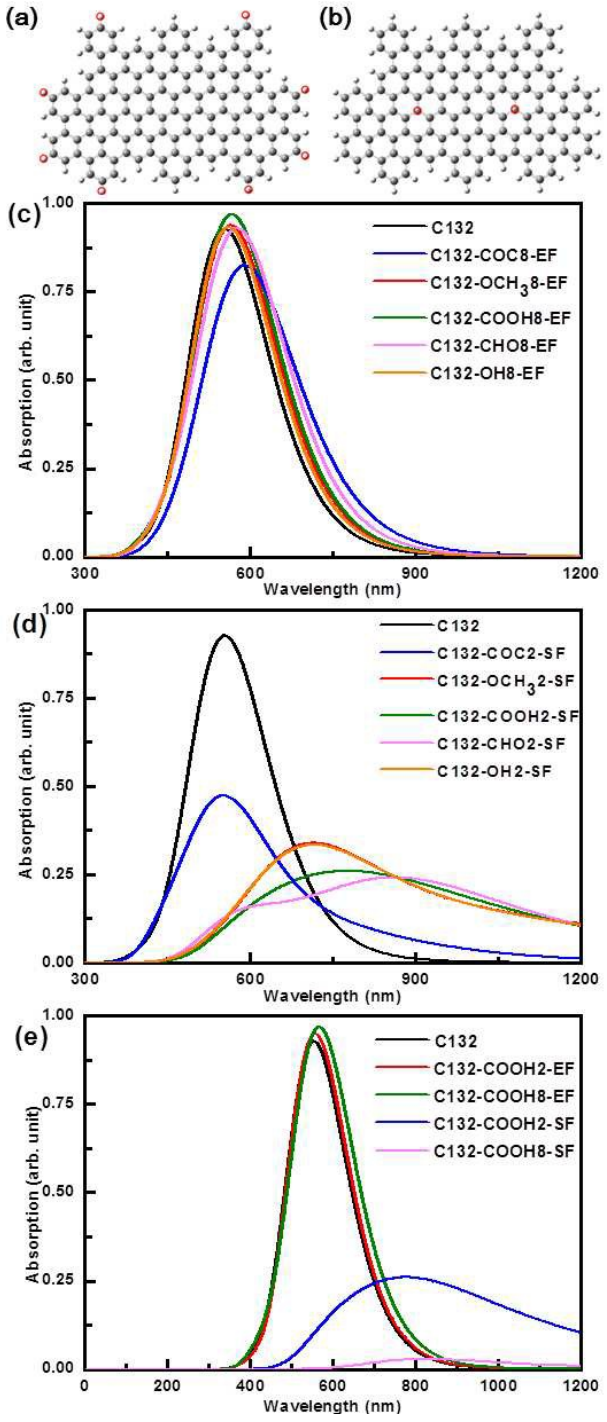

Fig. 1 (a) Edge functionalization position and (b) surface functionalization position of the GQDs, marked as red circles. The marked hydrogens are replaced by different functional groups and the marked carbons are attached with these functional groups. (c)-(e) The calculated absorption spectra of the GQDs with different types and number of oxygen-containing groups.

View Article Online
DOI: 10.1039/C7TC00631D

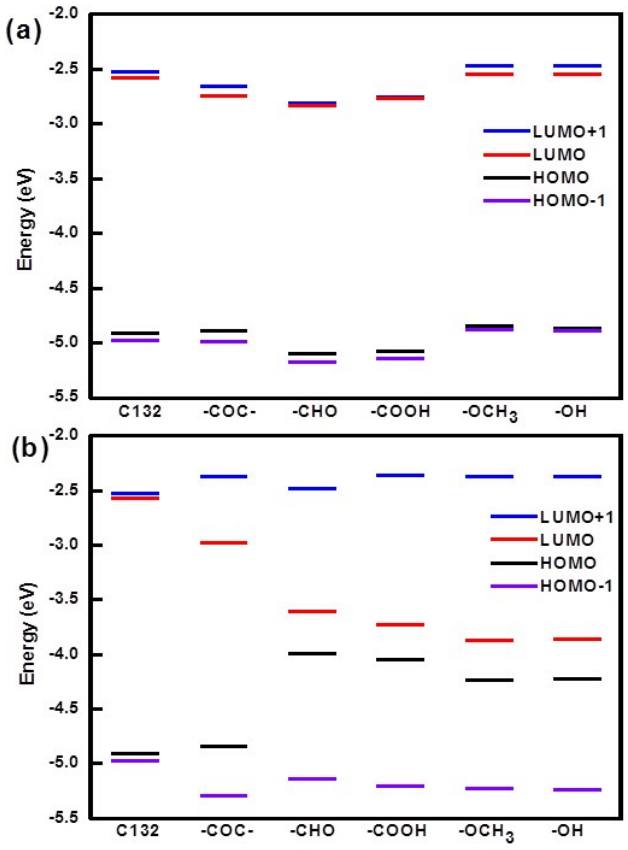

Fig. 2 Energy diagrams of GQDs with different oxygen-containing groups, (a) edge-functionalized GQDs and (b) surface-functionalized GQDs. The predicted energy levels corresponding to HOMO-1, HOMO, LUMO and LUMO+1 are shown for all GQDs.

The absorption spectra of GQDs are determined with the energy levels of the highest occupied molecular orbitals (HOMO) and the lowest unoccupied molecular orbitals (LUMO). Thus, the predicted energy levels corresponding to HOMO-1, HOMO, LUMO and LUMO+1 in Fig. 2 are depicted to reveal effects of different positions of various oxygen-containing groups in GQDs. As shown in Fig. 2, the HOMO–LUMO gap levels can be continuously tuned with different oxygen-containing groups as a consequence of orbital interactions. In general, electron-donating groups such as -COC-, -OH, and-OCH_3 increase the HOMO energy, while electron-withdrawing groups such as -CHO and -COOH lower the LUMO energy, resulting in a decreased HOMO–LUMO gap. Energy gap tunability is demonstrated in a clear red shift of absorption edges with narrowing of the HOMO–LUMO gap. However, compared with Fig. 2a and Fig. 2b, the HOMO–LUMO gap reduction of oxygen-containing groups located on the surface plane are more observable than that of substitutions on the edge plane. As shown in Fig. 2a, the calculated HOMO–LUMO gap of pristine GQDs and functionalized GQDs with -OH, -COOH, -OCH_3, -CHO, and -COC- are 2.34, 2.32, 2.31, 2.30, 2.27, and 2.15 eV, respectively. Therefore, the effect of oxygen functional groups located on the edge plane in GQDs is minor. Moreover, the calculated HOMO–LUMO gap of edge-functionalized GQDs is C132-OH8-EF > C132-COOH8-EF > C132-$OCH_3$8-EF > C132-CHO8-EF > C132-COC8-EF. The HOMO–LUMO gap of surface-functionalized GQDs with -OH, -COOH, -OCH3, -CHO, and -COC- are 0.36, 0.32, 0.37, 0.39, and 1.86 eV, respectively. The calculated HOMO–LUMO gap is C132-COC2-SF > C132-CHO2-SF > C132-$OCH_3$2-SF > C132-OH2-SF > C132-COOH2-SF. It is worth noting that the calculated HOMO–LUMO gaps of surface- and edge-functionalized GQDs are almost opposite. It can be speculated that the functional group in edge-functionalized GQDs is not the main factor for tuning the HOMO–LUMO gap of GQDs. For instance, the investigation on electronic gap reduction in edge-functionalized GQDs revealed that functionalization-induced distortions contribute to the observed lowering by about 35–55 %.[50] To determine the main factor for the surface functionalization in GQDs, we substitute the two oxygen functional groups with hydrogens in the surface-functionalized GQDs. The HOMO-LUMO gap of C132-H2-SF with geometry relaxation is 0.28 eV， which is close to the value of surface-functionalized GQDs from 0.32 to 0.39 eV except for C132-COC2-SF. This indicates that the effect of geometry distortion in surface-functionalized GQDs is the dominating factor for tuning the HOMO–LUMO gap of GQDs. As can be seen from the absorption spectra in Fig. 1d and the HOMO-LOMO gaps in Fig.2b, particularly, the -COC- group behaves significantly different from the other four functional groups in surface-functionalized GQDs, which is discussed later.

Another important factor of energy gap reduction is consistent with frontier orbital hybridization where a larger hybridization indicates a larger reduction. In order to study the frontier orbital hybridization of the GQDs, the isosurfaces of HOMO and LUMO are plotted in Fig. 3. As shown in Fig. 3a, the HOMO and LUMO of pristine GQDs obviously delocalize on the face of the carbon skeleton, and form a big π bond conjugate system. Moreover, the profiles of HOMO and LUMO orbitals of pristine GQDs show symmetry about mirrors. In order to gain insight into the optical mechanism of pristine and functionalized GQDs, we also depict the HOMO and LUMO of functionalized GQDs with different oxygen-containing groups. In this section, we take the functionalized GQDs with -COOH and -COC- as examples, and the other functionalized GQDs exhibit similar orbitals (as given in Fig. S3 in SI). As shown in Fig. 3b and 3d, the contours of HOMO and LUMO in edge-functionalized GQDs are similar to those in pristine GQDs. The above discussions also suggest that absorption spectra and HOMO–LUMO gaps have a slight change between pristine and edge-functionalized GQDs. Generally speaking, the closer the frontier orbital energies of GQDs, the greater the similarity of the corresponding spatial distribution of wave functions. It is quite apparent that optical properties of GQDs have an intimate relation with the electron structures of GQDs. In Fig. 3c and 3e, the contours of HOMO and LUMO in surface-functionalized GQDs are extremely different from those in pristine GQDs, leading to an obvious change of absorption spectra and HOMO–LUMO gaps in surface-functionalized GQDs. A comparison of frontier molecular orbital isosurfaces of C132-COOH2-SF and C132- COC2-SF in Fig. 3c and 3e shows that surface functionalization results in an obvious decrease of the delocalization in the HOMO and LUMO, and lower symmetry of orbitals is observed. For example, the HOMOs of the pristine GQDs and C132-COOH2-SF are similar, whereas

View Article Online
DOI: 10.1039/C7TC00631D

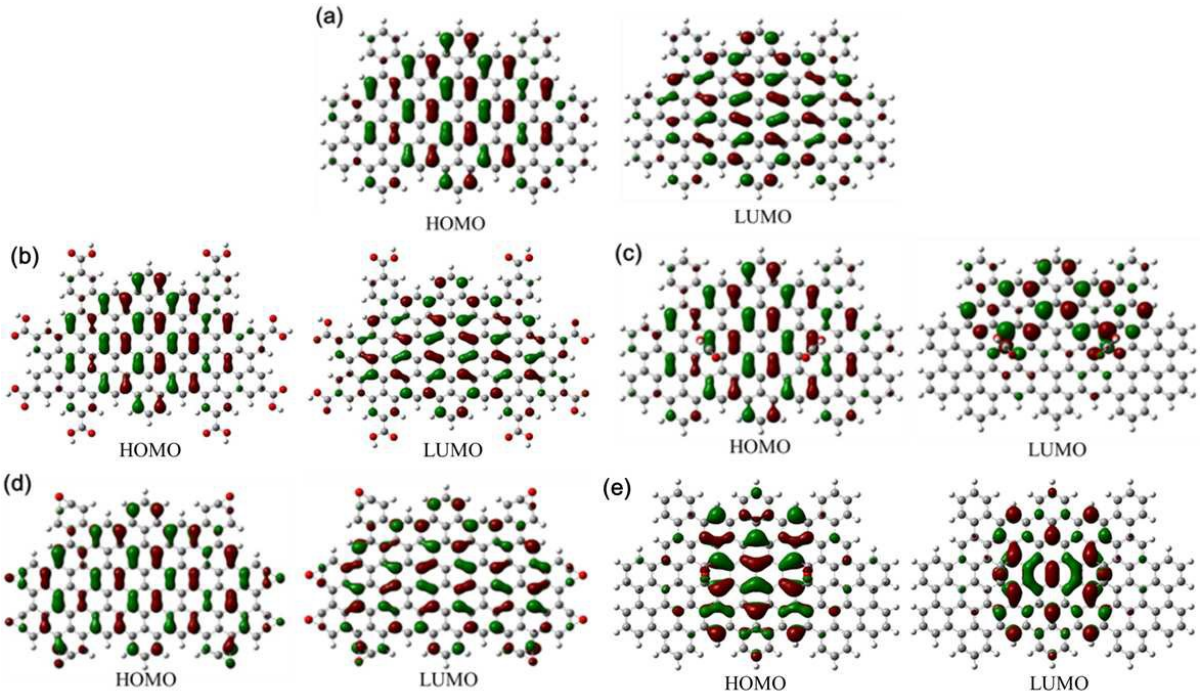

Fig. 3 Isosurfaces of HOMO and LUMO in GQDs with different oxygen-containing groups in ground state. The positive and negative orbital lobes are displayed in red and green colors, respectively. (a) pristine GQD, (b) C132-COOH8-EF, (c) C132-COOH2-SF, (d) C132-COC8-EF, and (e) C132-COC2-SF.

the LUMO of C132-COOH2-SF is greatly different from that of pristine GQDs, as presented in Fig. 3a and 3c. The HOMO and LUMO of pristine GQDs have clear π properties. Nevertheless, the HOMO of C132-COOH2-SF has clear π property, and LUMO has the property of σ orbit. Hence, the maximum absorption of C132-COOH2-SF may be not dominated by π(HOMO) → π*(LUMO) transition, the details of which will be discussed below. As we know, an ideal graphene sheet consists entirely of sp^2 hybridized carbon atoms. In carbon materials containing a mixture of sp^2 and sp^3 bonding, the optoelectronic properties are determined by the π states of the sp^2 sites. The π and π* electronic levels of the sp^2 clusters lie within the energy gap of σ and σ* states of the sp^3 matrix and strongly localized. As presented in Fig. 3c and 3e, the carbon in the basal plane could change from sp^2 hybridization to sp^3 hybridization through σ bonding with oxygen or carbon in the form of oxygen-containing groups, which alter the absorption spectra and HOMO–LUMO gap of functionalized GQDs. Chien et al.[51] proposed that the presence of isolated sp^2 clusters within the carbon–oxygen sp^3 matrix is responsible for the PL arising from graphene oxide sheets. It is expected that electrical and optical properties of GQDs can be tuned by tuning the sp^3 fraction based on controlling the quantity and location of oxygen-containing groups in GQDs.

In general, it would be challenging to keep GQDs molecular structure in symmetrically paired or mirror image forms in experiments. Hence, another edge position and the other four surface positions without symmetry are chosen to study their optical properties. The detail of positions and calculation results are given in Fig. S4-S8 and Table S12 (SI). These calculations show a strong effect of the position of oxygen groups on optical properties. Both edge and surface functionalization with oxygen groups reduces the HOMO–LUMO gap compared with the values of their corresponding pristine GQDs. For -COOH group based surface-functionalized GQDs, the HOMO–LUMO gap depends significantly on the position of the functionalization. In general, the absorption maximum wavelengths are shifted to the red, but a few substitution positions show small shift or blue shift. These differences are related to the reordering of the orbitals because of functionalization and the creation of hybridization, as shown in the isosurfaces of HOMO and LUMO in Fig. S8 (SI). It indicates that selective position functionalization offers a strategy to tune optical and electronic properties.

DFT method calculates virtual and occupied molecular orbitals (MOs) in ground state being suitable mainly for a crude evaluation of electronic transition energies such as the trends related to their changes in a solvent environment. However, characterizing specific transitions associated with an excited state is straightforward. Another helpful technique is to examine natural transition orbitals (NTOs).[52] These orbitals can be rapidly computed using transition densities produced by time-dependent energy calculations. NTOs are a transformed version of the canonical orbitals that attempt to isolate a specific excited state transition to one or two pairs of orbitals and describe the most important features of a transition. As opposed to state density, it is impossible to diagonalize transition density since it is not symmetric. However, a singular value decomposition scheme can be used where the decomposition of transition density matrix using unitary matrices U and V may be written as

View Article Online
DOI: 10.1039/C7TC00631D

Table 2 Excitation energies, wavelengths, oscillator strengths, transition coefficients, and associated eigenvalues of the dominated excitation in GQDs.

GQDs	Dominated excitation	Excitation energy(eV)	Wavelength (nm)	Oscillator strength(f)	Transition coefficients	Associated eigenvalues(λ_i)
C132	S3	2.21	559.83	3.22	H-1 → L 0.51	0.53
					H → L+1 -0.49	0.47
C132-COC8-EF	S3	2.06	601.53	2.81	H-1 → L 0.50	0.51
					H → L+1 0.49	0.49
C132-COOH8-EF	S3	2.16	573.47	3.32	H-1 → L 0.54	0.59
					H → L+1 -0.45	0.41
C132-COC2-SF	S5	2.23	556.63	2.00	H-1 → L 0.30	0.79
					H → L+2 0.63	0.20
C132-COOH2-SF	S6	1.53	812.15	0.60	H-4 → L -0.31	
					H-2 → L -0.15	0.76
					H → L+2 0.60	0.24
					H → L+3 0.11	

$$D^{0I}=U\,\mathrm{diag}\left(\sqrt{\lambda_1},\sqrt{\lambda_2},\ldots\right)V^{T}$$

Where U denotes a set of initial (hole) orbitals and V the final (electron) orbitals, λ_i is the associated eigenvalue reflecting the importance of a particular particle-hole excitation to the overall transition, and the superscripts 0, I are used for ground and Ith excited states. We focus on dominated excited states in GQDs, which play an important role in the absorption process due to their largest oscillator strengths. As shown in Table 2, orbital transition coefficients for the most obvious contributions, excitation energy, wavelength, and oscillator strength to the dominated excitation are listed. In this section, we choose the functionalized GQDs with -COOH and -COC- as examples, and the other functionalized GQDs' coefficients are listed in Tables S13 in SI. No one transition clearly dominates, and examining the relevant canonical orbitals is not particularly helpful in these states. It is clearly noticed that the states are described by a substantial list of orbital transitions. For example, the dominated transition in pristine GQDs is from S0→S3, and is a mixed transition between H-1→L (52.09%) and H→L+1 (47.17%), where H and L indicate the HOMO and LUMO orbitals and the bracketed data indicates the orbital transition contribution. Compared with other dominated excitation of edge-functionalized GQDs, it is noted that they have the same pattern of orbital transition, and the orbital transition contributions are similar. However, orbital transition coefficients of surface-functionalized GQDs are similar in magnitude, without a clear dominant component. In Table 2, it is evident that the maximum absorption for C132-COOH2-SF occurs at the excitation energy 1.53 eV, with oscillator strength f = 0.60. It represents a transition from S0→S6, and is a mixed transition between H-4→L (19.32%), H-2→L (4.64%), H→L+2 (71.43%), and H →L+3 (2.34%). As can be seen from the mix transition, the maximum absorption of C132-COOH2-SF is not dominated HOMO→LUMO transition. Thus, examining the relevant canonical orbitals is not particularly helpful in the excitation state. The NTOs corresponding to the most dominant singlet transitions for GQDs are calculated by TD-DFT method, and the corresponding associated eigenvalues are obtained and listed in Table 2. The excited state can be expressed with two pairs of orbitals by transforming the ordinary orbital representation into a more compact form. Fig. 4 illustrates the NTOs corresponding to the most dominant singlet transitions of GQDs with the associated eigenvalues (functionalized GQDs with -COOH and -COC- are exhibited as examples, and the other functionalized GQDs are given in Fig. S9 in SI). The singlet excitations are completely expressed as multiple sets of NTOs. As shown in Fig. 4a, the extent of electron delocalization in pristine GQDs with S0→S3 transition is described by the two pairs of NTOs, the electron cloud in carbon skeleton. It indicates a higher electron delocalization. This trend continues for C132-COOH8-EF and C132-COC8-EF. It reveals that the alteration of electron structure is minute in edge-functionalized GQDs with oxygen-containing groups. However, for the hole and particle NTOs of surface-functionalized GQDs, the electron wavefunctions are more concentrated over partial regions, indicating a higher localization. The overlap between the hole NTOs and particle NTOs in C132-COC2-SF is smaller than that in C132-COOH2-SF, indicating a higher delocalization. Observing the NTOs of C132-COC2-SF from Fig. 4e, the electron cloud with λ_i=0.79 moves from the central and middle region and spreads throughout the structure, and the electron cloud with λ_i=0.20 moves from the external and middle region towards the middle region. Through a comprehensive consideration, it indicates that the electron delocalization of pristine GQDs is similar to that of edge-functionalized GQDs, and the electron delocalization of edge-functionalized GQDs is higher than that of surface-functionalized GQDs.

View Article Online
DOI: 10.1039/C7TC00631D

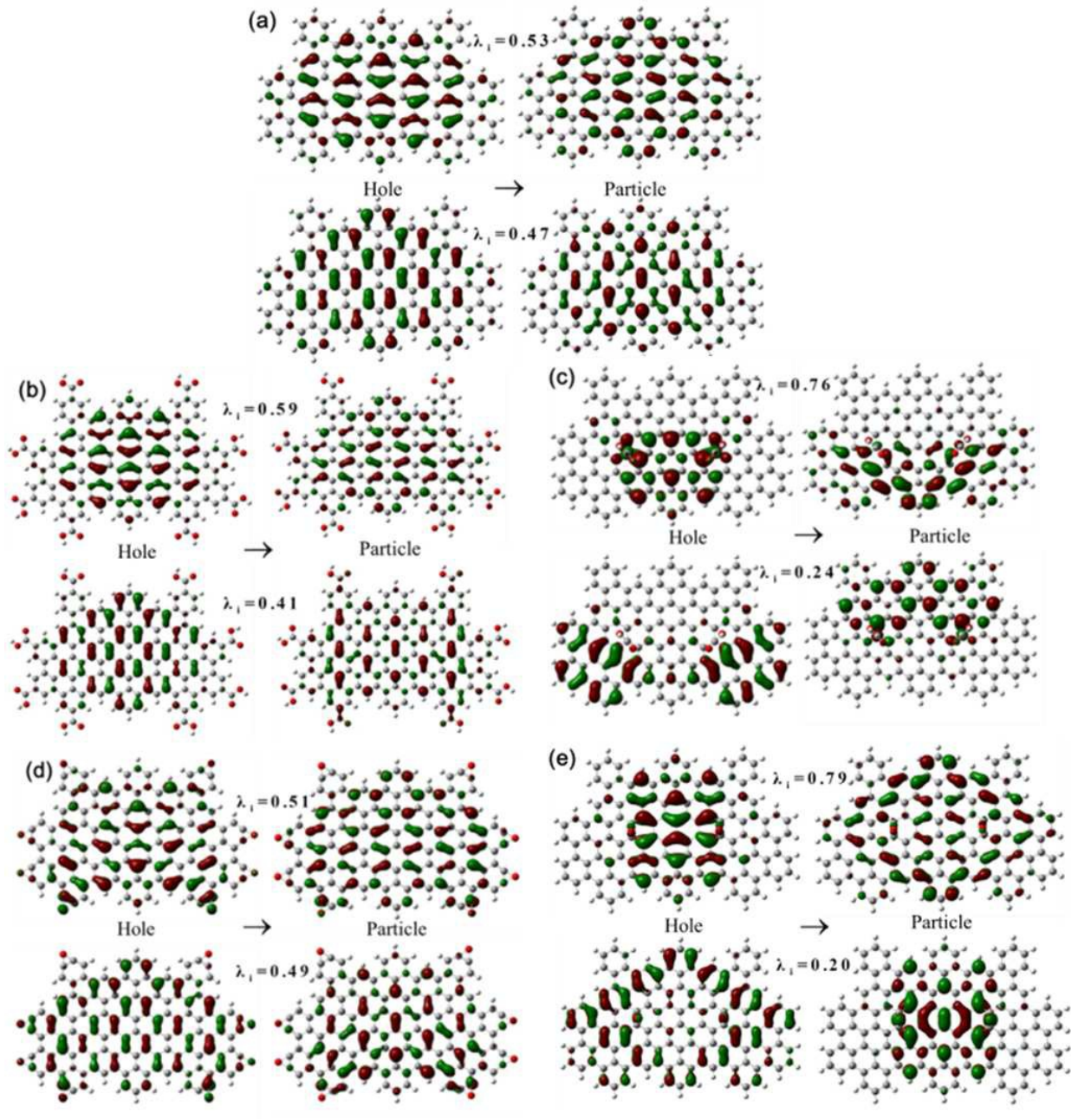

Fig. 4 NTO pairs for the dominant excited state of GQDs. For this state the "hole" is on the left, the "particle" is on the right; the values represent the associated eigenvalue (λ_i) of respective NTOs. (a) pristine GQD, (b) C132-COOH8-EF, (c) C132-COOH2-SF, (d) C132-COC8-EF, and (e) C132-COC2-SF.

Apart from the localization of sp^2 clusters, the mechanism of optical properties is also analysed based on charge transfer. A proper description of charge transfer states is very important for the analysis of the mechanism of optical properties. Difference densities are often a quite useful method of analyzing the transition corresponding to excited states. Thus, the combinations of the orbital-based method and the density-based ones together with the numerical results would give us clear interpretation of the excited state properties of GQDs. The following figures show the representations of difference density between the excited state minus the ground state (functionalized GQDs with -COOH and -COC- are exhibited as examples, and the other functionalized GQDs are given in Fig. S10 in SI). The yellow region indicates where the difference

View Article Online
DOI: 10.1039/C7TC00631D

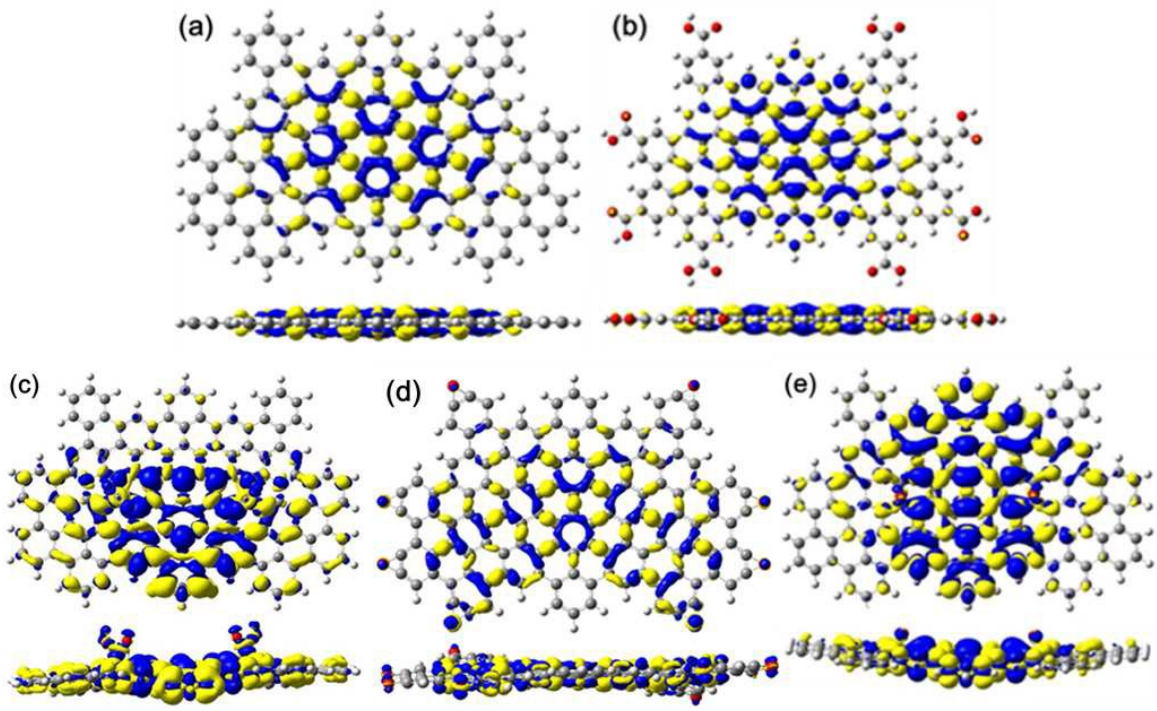

Fig. 5 Representation of the electron difference density between the dominated excited state minus ground state for GQDs. At the bottom, the lateral views are shown. (a) pristine GQD, (b) C132-COOH8-EF, (c) C132-COOH2-SF, (d) C132-COC8-EF, and (e) C132-COC2-SF. (The value of the difference density is ±0.0002).

density is positive, meaning that the electron density in the excited state is larger than that in the ground state. Electron density moves from the blue region to the yellow region when moving from the ground state to the excited state. Thus, for the most part, the transition can be described as a charge transfer originating from two areas. As shown in Fig. 5, the electron difference densities (EDD) reveal that the electron–hole pairs delocalize over the whole molecule and that the electrons transfer from adjacent holes. Thus, this electronic transition is locally excited. As shown in Fig. 5b and 5d, comparing the EDD of pristine GQDs, one can find that the delocalization of the electron–hole pair in edge-functionalized GQDs is similar to that in pristine GQDs. This shows that functionalization on the edge has a slight variation on the distribution of electron densities compared to pristine GQDs. In contrast, functionalization on the surface panel significantly changes the distribution of electron–hole pairs with respect to pristine GQDs, as shown in Fig. 5c and 5e. One can see that the electron–hole pairs in surface-functionalized GQDs are changed by the oxygen-containing groups, which may lead to radiative recombination of localized electron–hole pairs, and uneven distribution of electron–hole pairs resulting in asymmetric variations of electron structure in GQDs. For example, the electrons–hole pairs in C132-COOH2-SF are not significantly separated, and the degree of electron transfer from holes is weak because of strong interaction between electrons and holes in electronic transitions. Such oxygen-containing groups with finite number of atoms have decreased HOMO–LUMO gaps and provide confinement for electron–hole pairs created by absorption of photons. It has been proposed that the GQDs commonly contain carboxylic and epoxide groups, which can act as the non-radiative electron–hole recombination centers.[53] The plots of the EDDs show that functionalization on the basal plane plays an important role on changing the distribution of electron densities in surface-functionalized GQDs. In contrast, functionalization on the edge positions does not significantly change the distribution of the electron densities with respect to pristine GQDs. Due to the involvement of oxygen functional groups, the deformation of the geometry is the evident reason to explain how surface functionalization affects absorption spectra and HOMO–LUMO gap more obviously than edge functionalization.

In the above discussion about the absorption spectra and the HOMO–LUMO gap, it has been found that the -COC- behaves significantly different from the other functional groups in surface-functionalized GQDs. As we know, the binding of oxygen functional groups perturbs the electronic structure of GQDs by destroying local π-electron states. The -COC- can be regarded as a double-site impurity, while the other four groups are regarded as single-site impurities on the GQDs. A single oxygen functional group on GQDs can induce significant local distortion. A -COC- has one oxygen atom bridging over two neighbouring carbon atoms. The relaxed C-C bond length between the two carbon atoms bonded with the oxygen atom is 1.52 Å, larger than the C-C bond length in pristine GQDs (1.42 Å), but very close to that in ethane with

View Article Online
DOI: 10.1039/C7TC00631D

sp^3-sp^3 bonding (1.54 Å). Similarly, the averaged C-C bond length of the carbon atom connected to the -COOH with three nearest-neighbour carbon atoms is also 1.52 Å. These representations show that the surface-functionalized GQDs hinged by -COC- keep their planar sp^2 structure very well, and the delocalization of π-electron in surface-functionalized GQDs with -COC- is maintained.

It is important to note that the absorption spectra and the HOMO–LUMO gap have intimate relationships with electronic states. Compared with Fig. 4 and Fig. 5, the difference between the -COC- and -COOH in surface-functionalized GQDs are obvious for NTO and EDD representation. As can be seen in Fig. 4c and 4e, the distribution of the hole and particle NTOs in C132-COC2-SF is less disorder than that in C132-COOH2-SF. It indicates that the effect of the -COC- on electron transition is less intensive than that of the -COOH in surface functionalized GQDs. As shown in Fig. 5c and 5e, the distortion of electron densities in surface-functionalized GQDs with -COC- is negligible, while that of electron densities in GQDs with -COOH is evident. It has been suggested that there is an important role of the functional groups in the HOMO–LUMO gap reduction of GQDs. A mechanism based on the competition and collaboration between frontier orbital hybridization and charge transfer is proposed.[39] The frontier orbital hybridization of the GQD moiety and functional group reduces the HOMO–LUMO gap, while the charge transfer from the GQD moiety to the functional group enlarges it. These calculations show a more significant difference for the -COC- than that of the other four functional groups on the electronic properties and the HOMO–LUMO gaps. As shown in Fig. 5e, the delocalization of the electron–hole pair in C132-COC2-SF GQDs is similar to that in pristine GQDs. For the oxygen functional groups, it is easy to observe hole densities around oxygen atoms in –COC-, while the distributions of electron–hole densities are alternating change in -COOH, as shown in Fig. 5c and 5e from the lateral views. It indicates that the dominated excited state is a charge transfer from the GQD moiety to the -COC- in C132-COC2-SF GQDs, while the dominated excited state is locally excited around -COOH in C132-COOH2-SF GQDs. Hence, the small charge transfer in C132-COC2-SF GQDs can interpret the reason that the HOMO–LUMO gap of C132-COC2-SF GQDs is higher than that of C132-COOH2-SF GQDs.

Conclusions

In order to elucidate the underlying absorption mechanism of GQDs, we have used the TD-DFT approach to investigate optical and electronic properties of GQDs with five oxygen-containing groups. The absorption spectra and the HOMO–LUMO gaps are calculated, where the calculated absorption maximum wavelength of pristine GQDs is consistent with experimental data. Edge-functionalization effect analysis shows that oxygen-containing groups on GQDs induce a small effect on optical and electronic properties whereas a large effect occurs when the basal planes of GQDs are decorated. The calculated HOMO–LUMO gap trends of surface- and edge-functionalized GQDs with five oxygen-containing groups are almost in the opposite order. Electron–hole coherence and exciton delocalization of charge transfer upon electronic transitions are investigated with the three-dimensional real space representations (NTOs and EDDs) for GQDs with different oxygen-containing groups. We find that the electronic transition of GQDs is locally excited, and the oxygen-containing groups in surface-functionalized GQDs lead to uneven distribution of the electron density and reduce the electron localization of GQDs. In addition, it is found that the epoxy group behaves significantly different from the other functional groups in optical mechanism of surface functionalized GQDs. It indicates that the oxygen functional groups play an important role in the optical mechanism of GQDs. It is expected that this work will provide valuable knowledge for understanding absorption mechanism and electronic properties of GQDs and designing new functionalized GQDs with oxygen-containing groups for further exploitation of desired applications.

Acknowledgements

This work was partially supported by the National Natural Science Foundation of China (51373086 and 51472174), the International Science & Technology Cooperation Program of China (2014DFA60150), the Department of Science and Technology of Shandong Province (2016GGX104010), the Department of Education of Shandong Province (J16LA14), and the Chemcloudcomputing of National Supercomputing Center in Shenzhen (Shenzhen Cloud Computing Center). L. F. Dong also thanks financial support from the Malmstrom Endowment Fund at Hamline University.

References

1. B. C. Martindale, G. A. Hutton, C. A. Caputo and E. Reisner, *J. Am. Chem. Soc.*, 2015, **137**, 6018–6025.
2. S. Zhu, Y. Song, X. Zhao, J. Shao, J. Zhang and B. Yang, *Nano Res.*, 2015, **8**, 355–381.
3. X. T. Zheng, A. Ananthanarayanan, K. Q. Luo and P. Chen, *Small*, 2015, **11**, 1620–1636.
4. Y. Du and S. Guo, Nanoscale, 2016, 8, 2532-2543
5. L. Li and X. Yan, *J. Phys. Chem. Lett.*, 2010, **1**, 2572–2576.
6. L. L. Li, J. Ji, R. Fei, C. Z. Wang, Q. Lu, J. R. Zhang, L. P. Jiang and J. J. Zhu, *Adv. Funct. Mater.*, 2012, **22**, 2971–2979.
7. S. Y. Lim, W. Shen and Z. Gao, *Chem. Soc. Rev.*, 2015, **44**, 362–381.
8. M. Bacon, S. J. Bradley and T. Nann, *Part. & Part. Syst. Char.*, 2014, **31**, 415–428.
9. L. A. Ponomarenko, F. Schedin, M. I. Katsnelson, R. Yang, E. W. Hill, K. S. Novoselov and A. K. Geim, *Science*, 2008, **320**, 356–358.
10. S. Zhu, J. Zhang, C. Qiao, S. Tang, Y. Li, W. Yuan, B. Li, L. Tian, F. Liu and R. Hu, *Chem. Commun.*, 2011, **47**, 6858–6860.

View Article Online
DOI: 10.1039/C7TC00631D

11. J. Moon, J. An, U. Sim, S. P. Cho, J. H. Kang, C. Chung, J. H. Seo, J. Lee, K. T. Nam and B. H. Hong, *Adv. Mater.,* 2014, **26**, 3501–3505.
12. V. Gupta, N. Chaudhary, R. Srivastava, G. D. Sharma, R. Bhardwaj and S. Chand, *J. Am. Chem. Soc.*, 2011, **133**, 9960–9963.
13. H. Tetsuka, A. Nagoya, T. Fukusumi and T. Matsui, *Adv. Mater.*, 2016, **28**, 4632–4638
14. M. Zhang, L. Bai, W. Shang, W. Xie, H. Ma, Y. Fu, D. Fang, H. Sun, L. Fan and M. Han, *J. Mater. Chem.*, 2012, **22**, 7461–7467.
15. W. Kwon, Y. H. Kim, C. L. Lee, M. Lee, H. C. Choi, T. W. Lee and S. W. Rhee, *Nano Lett.*, 2014, **14**, 1306–1311.
16. Y. Dong, C. Chen, X. Zheng, L. Gao, Z. Cui, H. Yang, C. Guo, Y. Chi and C. M. Li, *J. Mater.s Chem.*, 2012, **22**, 21776–21776.
17. J. Peng, W. Gao, B. K. Gupta, Z. Liu, R. Romeroaburto, L. Ge, L. Song, L. B. Alemany, X. Zhan and G. Gao, *Nano Lett.*, 2012, **12**, 844–849.
18. R. Ye, C. Xiang, J. Lin, Z. Peng, K. Huang, Z. Yan, N. P. Cook, E. L. Samuel, C. C. Hwang and G. Ruan, *Nat. Commun.*, 2013, **4**, 94–105.
19. D. Pan, J. Zhang, Z. Li and M. Wu, *Adv. Mater.*, 2010, **22**, 734–738.
20. J. Shen, Y. Zhu, C. Chen, X. Yang and C. Li, *Chem. Commun.*, 2011, **47**, 2580–2582.
21. J. Zong, Y. Zhu, X. Yang, J. Shen and C. Li, *Chem. Commun.*, 2010, **47**, 764–766.
22. H. Tetsuka, R. Asahi, A. Nagoya, K. Okamoto, I. Tajima, R. Ohta and A. Okamoto, *Adv. Mater.*, 2012, **24**, 5333–5338.
23. A. Ananthanarayanan, X. Wang, P. Routh, B. Sana, S. Lim, D. H. Kim, K. H. Lim, J. Li and C. Peng, *Adv. Funct. Mater.*, 2014, **24**, 3021–3026.
24. Z. Fan, Y. Li, X. Li, L. Fan, S. Zhou, D. Fang and S. Yang, *Carbon*, 2014, **70**, 149–156.
25. S. Zhuo, M. Shao and S. T. Lee, *Acs Nano*, 2012, **6**, 1059–1064.
26. X. Yan, X. Cui and L. S. Li, *J. Am. Chem. Soc.*, 2010, **132**, 5944–5945.
27. K. Habiba, V. I. Makarov, J. Avalos, M. J. Guinel, B. R. Weiner and G. Morell, *Carbon*, 2013, **64**, 341–350.
28. S. H. Jin, D. H. Kim, G. H. Jun, S. H. Hong and S. Jeon, *Acs Nano*, 2013, **7**, 1239–1245.
29. C. Sun, F. Figge, J. A. Mcguire, Q. Li and L. S. Li, *Phys.l Rev. Lett.*, 2014, **113**, 368–390.
30. L. Li, G. Wu, G. Yang, J. Peng, J. Zhao and J. J. Zhu, *Nanoscale*, 2013, **5**, 4015–4039.
31. L. Wang, S. J. Zhu, H. Y. Wang, S. N. Qu, Y. L. Zhang, J. H. Zhang, Q. D. Chen, H. L. Xu, W. Han and B. Yang, *Acs Nano*, 2014, **8**, 2541–2547.
32. S. Zhu, L. Wang, B. Li, Y. Song, X. Zhao, G. Zhang, S. Zhang, S. Lu, J. Zhang and H. Wang, *Carbon*, 2014, **77**, 462–472.
33. I. P. Hamilton, B. Li, X. Yan and L. Li, *Nano Lett.*, 2011, **11**, 1524–1529.
34. S. Zhu, J. Zhang, S. Tang, C. Qiao, L. Wang, H. Wang, X. Liu, B. Li, Y. Li and W. Yu, *Adv. Funct. Mater.*, 2012, **22**, 4732–4740.
35. R. Sekiya, Y. Uemura, H. Naito, K. Naka and T. Haino, *Chem.- Eur. J.*, 2016, **22**, 8198–8206.
36. S. Schumacher, *Phys. Rev. B Condens. Matter*, 2011, **83**, 3002–3005.
37. M. Zhao, F. Yang, Y. Xue, D. Xiao and Y. Guo, *Chem.Phys.Chem.*, 2014, **15**, 950–957.
38. K. R. Geethalakshmi, Y. N. Teng and R. Crespootero, *J.Mater. Chem. C*, 2016, **4**, 8429–8438.
39. Y. Li, H. Shu, X. Niu and J. Wang, *J.Phys. Chem. C*, 2015, **119**, 24950–24957.
40. A. D. Laurent and D. Jacquemin, *Int. J. Quantum Chem.*, 2013, **113**, 2019–2039.
41. J. Tomasi, B. Mennucci and R. Cammi, *ChemInform*, 2005, **36**, 2999–3093.
42. M. Cossi and V. Barone, *J. Chem. Phys.*, 2001, **115**, 4708–4717.
43. J. P. Cerón-Carrasco, D. Jacquemin, C. Laurence, A. Planchat, C. Reichardt and K. Sraïdi, *J. Phys. Chem. B*, 2014, **118**, 4605–4614.
44. H. Riesen, C. Wiebeler and S. Schumacher, *J. Phys. Chem. A*, 2014, **118**, 5189–5195.
45. M. J. Frisch, G. W. Trucks, H. B .Schlegel, et al. Gaussian 09, revision D. 01. 2009.
46. R.Dennington, T.Keith, J.Millam, et al. GaussView, version 5;Semichem Inc.: Shawnee Mission, KS, 2009.
47. J. W. Patterson. *J Am. Chem. Soc.*, 1942, **64**, 1485–1486
48. E. Clar and W. Schmidt, *Chem. Inform.*, 1977, **33**, 2093–2097.
49. C. Cocchi, D. Prezzi, A. Ruini, M. J. Caldas and E. Molinari, *J.Phys.Chem.C*, 2012, **116**, 17328–17335.
50. C. T. Chien, S. S. Li, W. J. Lai, Y. C. Yeh, H. A. Chen, I. S. Chen, L. C. Chen, K. H. Chen, T. Nemoto and S. Isoda, *Angew. Chem. Int.l Edit.*, 2012, **51**, 6662–6666.
51. R. L. Martin, *J. Chem.l Phys.*, 2003, **118**, 4775–4777.
52. K. P. Loh, Q. Bao, G. Eda and M. Chhowalla, *Nature Chem.* 2010, **2**, 1015–1024.

View Article Online
DOI: 10.1039/C7TC00631D

Table of Contents Entry

Optical and Electronic Properties of Graphene Quantum Dots with Oxygen-Containing Groups: a Density Functional Theory Study